Title	Anion-Responsive Colorimetric and Fluorometric Red-Shift in Triarylborane Derivatives: Dual Role of Phenazaborine as Lewis Acid and Electron Donor
Author(s)	Aota, Nae; Nakagawa, Riku; de Sousa, Leonardo Evaristo et al.
Citation	Angewandte Chemie – International Edition. 2024, 63(24), p. e202405158
Version Type	VoR
URL	https://hdl.handle.net/11094/95797
rights	This article is licensed under a Creative Commons Attribution 4.0 International License.
Note	

GDCh

Research Articles

Angewandte
Chemie
International Edition
www.angewandte.org

Donor-Acceptor Systems | Hot Paper

How to cite: *Angew. Chem. Int. Ed.* **2024**, e202405158
doi.org/10.1002/anie.202405158

Anion-Responsive Colorimetric and Fluorometric Red-Shift in Triarylborane Derivatives: Dual Role of Phenazaborine as Lewis Acid and Electron Donor

Nae Aota, Riku Nakagawa, Leonardo Evaristo de Sousa, Norimitsu Tohnai,
Satoshi Minakata, Piotr de Silva,* and Youhei Takeda*

Abstract: Photophysical modulation of triarylboranes (TABs) through Lewis acid-base interactions is a fundamental approach for sensing anions. Yet, design principles for anion-responsive TABs displaying significant red-shift in absorption and photoluminescence (PL) have remained elusive. Herein, a new strategy for modulating the photophysical properties of TABs in a red-shift mode has been presented, by using a nitrogen-bridged triarylborane (1,4-phenazaborine: PAzB) with a contradictory dual role as a Lewis acid and an electron donor. Following the strategy, PAzB derivatives connected with an electron-deficient azaaromatic have been developed, and these compounds display a distinct red-shift in their absorption and PL in response to an anion. Spectroscopic analyses and quantum chemical calculations have revealed the formation of a tetracoordinate borate upon the addition of fluoride, narrowing the HOMO–LUMO gap and enhancing the charge-transfer character in the excited state. This approach has also been demonstrated in modulating the photophysical properties of solid-state films.

Introduction

Since triorganoboranes (R_3B) possess a vacant $2p_\pi$ orbital on the boron center, they exhibit pronounced Lewis acidity and have thus been widely employed in organic synthesis[1]
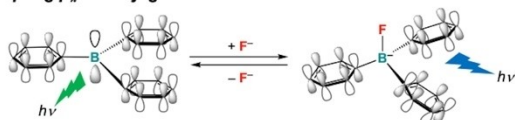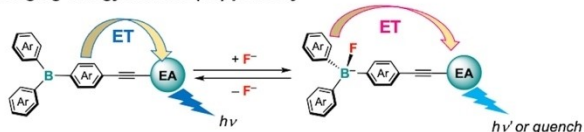
[*] N. Aota, R. Nakagawa, Prof. Dr. N. Tohnai, S. Minakata, Prof. Dr. Y. Takeda
Department of Applied Chemistry, Graduate School of Engineering
Osaka University
Yamadaoka 2-1, Suita, Osaka 565-0871, Japan
E-mail: takeda@chem.eng.osaka-u.ac.jp

Dr. L. E. de Sousa, Prof. Dr. P. de Silva
Department of Energy Conversion and Storage
Technical University of Denmark
Anker Engelunds Vej 301, 2800 Kongens Lyngby, Denmark
E-mail: pdes@dtu.dk

and catalysis.[2] Specifically, triarylboranes (TABs), which feature extended π-electron systems as the organic fragment (R=Ar), possess exceptional capability not only for accepting electrons but also for absorbing light in the near-ultraviolet to visible spectrum, owing to their delocalized π-systems spanning the entire molecule. As a result, TABs have been extensively utilized in materials science, finding a variety of applications such as electron transporting materials, nonlinear optical materials, and two-photon-excited fluorescent materials.[3]

In conjunction with intrinsic Lewis acidity and photo-absorbing capability, TABs offer substantial potential for modulating photophysical properties through Lewis acid-base interactions. The complexation of TABs with a Lewis base at the trivalent boron center perturbs their electronic structure, resulting in the breaking of conjugation, structural deformation, and an increase in electron density. By leveraging these phenomena, a wide array of TABs that are capable of sensing Lewis bases have been developed, which are typically classified into three distinct strategies (Figure 1a–c). Of particular importance is the detection of fluoride, as it has significant implications for healthcare and environmental pollution.[4] As a pioneering work in the field of TAB-based colorimetric sensing materials for fluoride, Yamaguchi and Tamao developed tris(9-anthryl)borane.[5] Upon complexation with fluoride, the p_π-π* conjugation between the anthracene units and the boron center is interrupted, resulting in a change in solution color from orange to colorless. A similar design approach based on the concept of "interrupting conjugation" (Figure 1a) has been applied to π-extended dibenzoboroles, which display a significant blue-shift of fluorescence in the visible light region upon the addition of fluoride and electron-donating solvent such as DMF.[6] Lewis base sensors based on TAB or its polymeric form in a "blue-shift" or "turn-off" mode have been most widely explored.[7–9] The binding event of fluoride to the electrophilic boron center offers an additional avenue for modulating photophysical properties through changing energy transfer (ET) pathway, resulting in a ratiometric change in both absorption and PL as illustrated in Figure 1b. Takeuchi and Shinkai have developed a conjugate of porphyrin and tris(durene)-cored TAB, with the porphyrin serving as the energy acceptor (EA) and the TAB serving as the energy donor (ED).[10] Inhibiting charge-transfer (CT) from an electron donor (D) to the TAB as an electronic acceptor (A) through complexation with a Lewis base is also

Angew. Chem. Int. Ed. **2024**, e202405158 (1 of 10)

© 2024 The Authors. Angewandte Chemie International Edition published by Wiley-VCH GmbH

Figure 1. a)–c) Previous strategies and d) our strategy for modulating the photophysical properties of TABs with fluoride. e) The HOMO/LUMO energies of **1-Mes** and its borate form [**1-Mes-2F**]$^{2-}$ estimated by DFT calculations.
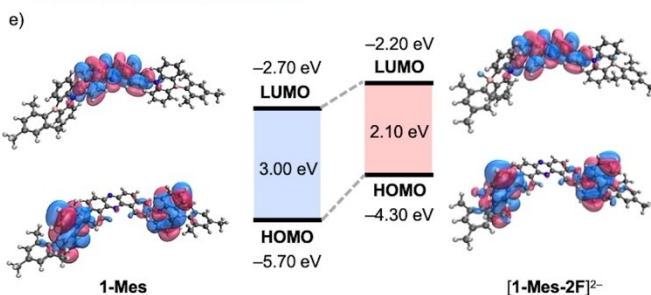
commonly utilized strategy for modulating the photophysical properties of TAB compounds, as illustrated in Figure 1c. Conjugated donor-π-acceptor (D–π–A) luminescent compounds, comprising TAB as the acceptor and triarylamines as the donor, exhibit a blue shift in PL wavelength upon coordination of fluoride to the boron center.[11,12]

The complexation with fluoride leads to a "blocking CT" mode and thus to an increase in the intensity of blue-shifted emission from the locally excited (LE) state of the donor. For example, Wang and co-workers reported on a D–π–A TAB compound that has an *N*-(1-naphthyl)phenylamino moiety as the donor and B(mesityl)$_2$ moiety as the acceptor, along with a 1,8-bis(4,4'-biphenyl)naphthalene unit as the π-linker, which exhibited green emission via through-space CT (TSCT) from the donor to the acceptor.[12] The green emission ratiometrically turned to blue with an increase in intensity as a function of the amount of fluoride added, as a result of the inhibition of TSCT (Figure 1c). By incorporating an extended π-system as the linker in the D–π–A system, multiple emission modes can be achieved through Lewis acid-base interactions (Figure 1c).[13] As mentioned above, the majority of known TABs exhibit a "blue-shift" of absorption and PL or "turn-off" of PL upon interaction with a Lewis base, mediated by the disruption of p$_\pi$-π* conjugation or the inhibition of CT (Figure 1a–c).[5–14] In sharp contrast, TABs that exhibit a red-shift of absorption and/or PL in response to a Lewis base, such as fluoride and cyanide, have been rarely explored, owing to the lack of rational

design principles for such materials.[15] Such anion-responsive TABs would offer new opportunities to detect anions in a complementary manner to hitherto reported materials.

Herein, we disclose the development of TAB compounds **1** (**1-Mes** and **1-Tipp**) that display a distinct red-shift in absorption and PL upon the interaction with a Lewis basic anion, which is enabled by a novel design strategy for narrowing the HOMO–LUMO energy gap and enhancing charge-transfer in the excited state through reversing the intrinsic role of TAB from an electronic acceptor to an electronic donor (as illustrated in Figure 1d).[16] More importantly, the substantial enhancement of CT in the excited states enables the red-shifting of emission even in solid-state host–guest systems, leading to modulation of PL in film state from blue to deep-red and near-infrared (NIR) region.

Results and Discussion

In order to endow a TAB compound with the contradictory dual role as a Lewis acid and an electronic donor, we designed orthogonally connected compounds comprising of two PAzBs and dibenzo[*a,j*]phenazine (DBPHZ), having different steric environments on boron atom [i.e., mesityl (Mes) and 2,4,6-triisopropylphenyl (Tipp) group (Figure 1d)]. Given that PAzB possesses a 14π-electron system, it serves as a B,N-analogue of anthracene[17a] and adopts a

planar structure.[17b,i] On one hand, the electronic resonance between the nitrogen and boron centers results in ambipolar electronic distribution (–N$^+$=C–C=B$^-$–); thus, the PAzB family exhibits distinct physicochemical properties.[17] We envisaged that the structural flatness and ambipolar electronic structure of PAzB would enable its utilization as an electron donor, given that the boron compound is connected with an appropriately electron-deficient unit. The introduction of a highly electron-deficient functional group, such as ammonium, phosphonium, and diarylboryl functionality, on the periphery of the PAzB unit drastically enhances binding constant (K) to the order of 10^5 M^{-1}, thereby enabling sufficient capture of fluoride in organic solvents.[18] We focused on DBPHZ as the electron-deficient unit, which exhibits a high electron affinity comparable to that of tris(8-hydroxyquinolinato)aluminum (Alq$_3$).[19] Additionally, the highly planar structure of DBPHZ and PAzB enables a perpendicular geometry of D and A units in a D–A–D architecture.[20] Thus, we hypothesized that the connection of PAzB and DBPHZ units increases the Lewis acidity of the trivalent boron center, due to a subsequent electron-withdrawing effect through the C–N σ single bond (i.e., inductive effect). Also, the orthogonal D–A–D structure would disconnect extended conjugation between D and A units, keeping the intrinsic Lewis acidity of the boron center. The Mes and Tipp groups were selected as the aryl moiety on the boron atom, due to the kinetic stabilization of the compounds.

The geometry optimization of the designed molecule **1-Mes** at the ground state, as determined by quantum chemical calculations based on density functional theory (DFT) at the LC-ωPBE level with the 6–31G(d,p) basis set, revealed that the PAzB adopts a completely planar structure, and the D–A–D molecule adopts a perpendicular geometry as anticipated (Figure 1e; for the detailed description on theoretical calculations, see the SI). It is worth noting that the HOMO and LUMO are localized on the PAzB and DBPHZ units, respectively (Figure 1e). This suggests that the PAzB serves as the electron donor in this molecular system, as designed. The HOMO–LUMO energy gap for its fluoride adduct [**1-Mes-2F**]$^{2-}$ (2.1 eV) was found to be narrower than that for **1-Mes** (3.0 eV) (Figure 1e), indicating the feasibility of red-shift of the absorption spectrum. Introduction of a larger aromatic group (Tipp) on the boron center (**1-Tipp**; [**1-Tipp-2F**]$^{2-}$) does not affect the HOMO/LUMO energy (–5.70 eV/–2.70 eV for **1-Tipp**; –4.30 eV/–2.20 eV for [**1-Tipp-2F**]$^{2-}$) and HOMO–LUMO gap (3.0 eV for **1-Tipp**; 2.1 eV for [**1-Tipp-2F**]$^{2-}$).

The syntheses of D–A–D compounds **1** are illustrated in [Eq. (S1–S4) and (S6–S8)]. The protection of the nitrogen atom of bis(2-bromophenyl)amine (**S1**) with a methoxymethyl (MOM) group was followed by lithium-bromine permutation and trapping the resulting dilithium species with MesB(OMe)$_2$ (**S3**)[21] and TippB(OMe)$_2$ (**S7**)[22] to afford N-MOM PAzB **S4** and **S8**, respectively [Eq. (S2) and (S6)]. Deprotection of the N-MOM group of **S4** and **S8** furnished donors **S5** and **S9**, respectively, in a high yield [Eq. (S3) and (S7)]. Phenazaborines **S5** and **S9** were then subjected to a Pd-catalyzed double Buchwald–Hartwig

amination with 3,11-dibromo-dibenzo[a,j]-phenazine (**S6**),[19] successfully yielding the target D–A–D compounds **1-Mes** and **1-Tipp**, respectively, in a high yield [Eq. (S4) and (S8)]. The compounds **1** were fully characterized by nuclear magnetic resonance (NMR) and infrared (IR) spectroscopy, mass spectrometry (MS), and elemental analysis (EA). Furthermore, all the ^{1}H and ^{13}C NMR signals of **1-Mes** were assigned by two-dimensional (2D) NMR spectroscopy (Figure S1–S3).

Single crystals of **1-Mes** and **1-Tipp** suitable for X-ray crystallographic diffraction analysis were grown from a biphasic solution (n-hexane/Et$_2$O for **1-Mes**; n-hexane/CHCl$_3$ for **1-Tipp**).[23] In both cases, the unit cell includes two independent molecules (Table S1; one of the molecules is shown in Figure 2a and b). The sum of the C–N–C bond angles [Σ(C–N–C)] and C–B–C bond angles [Σ(C–B–C)] are 359.8(0)°–360.0(0)° and 359.9(1)°–360.0(0)°, respectively (Figure 2a and b), indicating that the PAzB unit is planar. The B–C bond lengths within the PAzB ring [1.52-(6)–1.53(4) Å] are also in good agreement with previously reported PAzB compounds (Figure 2a and b).[17] The PAzB and DBPHZ planes are nearly orthogonal to each other [78.3(4)°–89.7(5)°, Figure 2a and b)], in agreement with the results of theoretical calculations. With regard to the geometry around the B center, the B-Mes and B-Tipp rings are also perpendicular to the PAzB plane (Figure 2a and b). While the U-shaped DBPHZ units are spatially isolated in the molecular packing structure of **1-Mes** (Figure 2c), **1-Tipp** forms an anti-parallel dimeric pairs with a close interplane distance of 3.40(3) Å (Figure 2d and inset Figure in Table S1). In the molecular packing structure, close C⋯H and C⋯N contacts were found (Figure S4).

To clarify the intrinsic photophysical properties of compounds **1** in a diluted solution, UV/Vis absorption and PL spectra were acquired in various solvents (CyH: cyclohexane, Tol: toluene, Diox: 1,4-dioxane, EtOAc: ethyl acetate, THF: tetrahydrofuran, CHCl$_3$: chloroform, Ace: acetone, and DMF: N,N-dimethylformamide) (Figure 3, Figure S5–S7; Table 1 and Table S2–S4). In all the solvents, compound **1-Mes** exhibited a strong and sharp absorption at around λ_{abs} 296 nm, as well as vibronic structured absorptions between λ_{abs} 350 and 450 nm (Figure 3). Comparison with the absorption spectrum of the individual D and A components and their mixture (D:A=2:1) in THF (Figure S8 and Table S5) revealed that the longest absorption maximum (λ_{abs}=419 nm) is attributed to the local excitation of the acceptor (λ_{abs}=416 nm). A more detailed examination of the absorption spectra revealed the presence of a tail band between 420 and 440 nm, which is not present in the spectrum of an admixture of D and A (D:A=2:1) (Figure S8). Thus, this observed new band in this regime is ascribed to an intramolecular charge-transfer (ICT) transition from the donor to the acceptor. The simulated absorption spectrum derived from the nuclear ensemble method[24] including 10 excited states displays similar behavior (Figure S12), with a main peak at 374 nm followed by a lower intensity tail at the 440 nm mark. Analysis of the absorption in the ensemble indicates that the S$_0$ to S$_1$ transitions are mainly localized in the acceptor unit, with
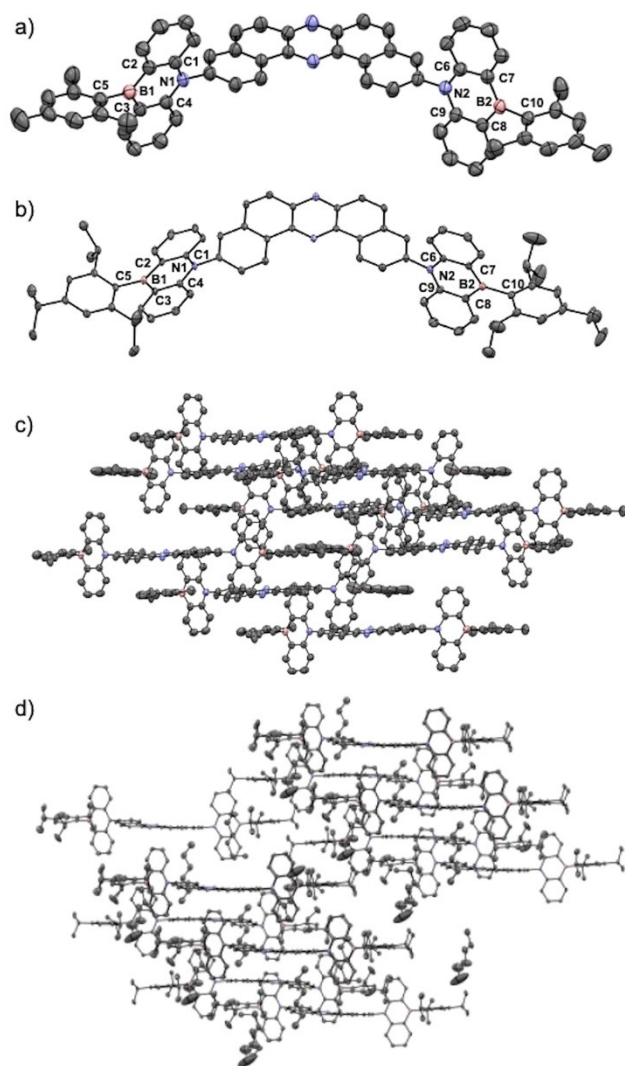
Figure 3. Steady-state UV/Vis and PL spectra of diluted solutions ($c = 10^{-5}$ M) of **1-Mes**. The absorption spectrum of acetone solution is cut off at 330 nm, due to the intense absorption of the solvent. The inset photograph and graph show the PL of each solution under the irradiation of a UV lamp ($\lambda_{ex} = 365$ nm) and the Lippert–Mataga plot, respectively.

Figure 2. Molecular geometry of a) **1-Mes** and b) **1-Tipp** in the single crystal; Molecular packing structure of c) **1-Mes** and d) **1-Tipp** in the single crystal. Thermal ellipsoids are set at the 50% probability level. Selected geometry parameters for **1-Mes**: [Σ(C–N1–C)] = 359.9(9)°; [Σ(C–N2–C)] = 360.0(0)°; [Σ(C–B1–C)] = 359.9(9)°, [Σ(C–B2–C)] = 359.9(1)°; N1–C1 = 1.40(1) Å; C1–C2 = 1.41(0) Å; C2–B1 = 1.53(0) Å; B1–C3 = 1.52(8) A; C3–C4 = 1.40(8) Å; C4–N1 = 1.39(4) Å; N2–C6 = 1.39(1) Å; C6–C7 = 1.41(3) Å; C7–B2 = 1.53(2) Å; B2–C8 = 1.52(9) Å; C8–C9 = 1.41(6) Å; C9–N2 = 1.40(6) Å. Selected geometry parameters for **1-Tipp**: [Σ(C–N1–C)] = 359.9(9)°; [Σ-(C–N2–C)] = 359.8(0)°; [Σ(C–B1–C)] = 360.0(0)°, [Σ(C–B2–C)] = 359.9-(4)°; N1–C1 = 1.39(6) Å; C1–C2 = 1.41(3) Å; C2–B1 = 1.52(6) Å; B1–C3 = 1.53(2) A; C3–C4 = 1.41(4) Å; C4–N1 = 1.39(3) Å; N2–C6 = 1.39(8) Å; C6–C7 = 1.41(4) Å; C7–B2 = 1.53(4) Å; B2–C8 = 1.53(0) Å; C8–C9 = 1.41(2) Å; C9–N2 = 1.39(7) Å.

occasional vibrationally-induced CT states being responsible for the lower energy absorption band (Figure S13).

Although the absorption spectra were not affected by the polarity of the organic solvent, the PL spectrum of **1-Mes** was drastically red-shifted as a function of solvent polarity, from the blue to the red region (i.e., positive solvatoluminochromism) (Figure 3). The Lippert–Mataga plot clearly shows a good linear correlation between the
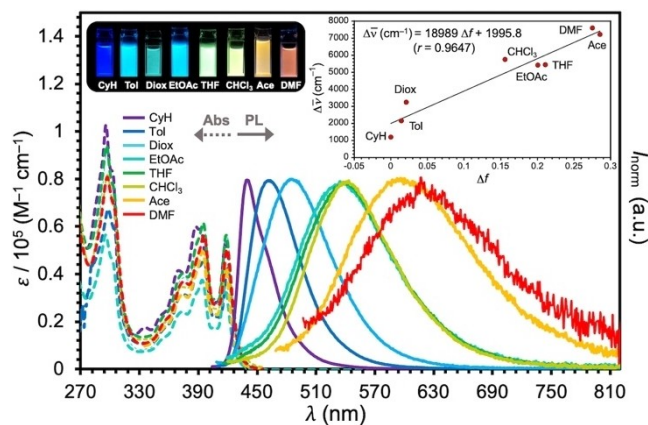
orientation polarizability of the solvent (Δf) and the Stokes shift (the inset graph in Figure 3). The dipole moment in the excited state, estimated from the Lippert–Mataga plot ($\mu_{ex} = 30.01$ Debye), is significantly higher than that in the ground state ($\mu_{g} = 2.59$ Debye). Furthermore, the emission from **1-Mes** is clearly different from the admixture of D and A (D:A = 2:1) (Figure S8), and its spectrum has a Gaussian-type broad shape, suggesting that the D–A–D compound **1-Mes** exhibits CT characteristics in the excited state. These results proved that the PAzB serves as a donor in the triad system. The alternation of the B-aryl group from Mes to a bulkier aryl group (**1-Tipp**) did not provide significant change in UV/Vis absorption and PL properties (Figure S5 and S7; Table S3 and S4).

Simulations for the emission spectrum of compounds **1** proved challenging. Excited state calculations predicted emission from excitations localized in the acceptor unit at around 515 nm. Being a localized excitation, it was insensitive to changes in solvent polarity. This combination resembles the observed emission in EtOAc, CHCl₃, and THF, which is solvent insensitive and peaks around 540 nm, but does not reproduce the emission in the remaining solvents. It indicates that other equilibrium geometry should exist, perhaps due to solvent interactions. In this sense, the use of an S₂ optimized geometry to produce a new ensemble revealed the existence of S₁ states with higher CT character with emission peaks at 419 nm in 1,4-dioxane and 427 nm in toluene, closer to the experimental results in low polarity solvents (Figure S14). This amount of red-shift is smaller than the observed experimentally, which indicates an underestimation of the strength of the CT states of compounds **1**. On the other hand, emission rates from simulated spectra of **1-Mes** are estimated at $(5.0 \pm 1.0) \times 10^{7}$ s⁻¹ in 1,4-dioxane and $(4.8 \pm 0.4) \times 10^{6}$ s⁻¹ in THF, which are consistent with the measured fluorescence rates (Table 1 and S4).

Importantly, the addition of a Lewis basic anion (20 equiv) to the THF solution of **1-Mes** drastically changed

Table 1: Summary of the photophysical properties of diluted solution of **1-Mes** ($c = 10^{-5}$ M).

Solvent	λ_{abs} (nm)	ε (M^{-1}cm^{-1})	λ_{em} (nm)[a]	Φ_{PL}[b]	$<\tau>$ (ns)[c]	k_f (s^{-1})[d]
CyH	388, 418	60000, 53000	440	0.23	1.43	1.61×10^8
Tol	396, 420	46000, 42400	463	0.26	3.38	7.69×10^7
Diox	395, 419	60500, 56500	485	0.23	6.25	3.68×10^7
EtOAc	394, 417	37400, 34300	539	0.11	10.19	1.08×10^7
THF	395, 419	61500, 56300	543	0.14	13.62	1.03×10^7
CHCl$_3$	395, 419	49900, 42700	552	0.13	10.23	1.27×10^7
Ace	394, 417	49500, 44100	597	0.08	15.00	5.33×10^6
DMF	396, 419	51400, 50500	617	0.02	3.72	5.38×10^6

[a] Excited at $\lambda_{ex} = 365$ nm. [b] The absolute photoluminescence quantum yield acquired with an integral sphere. [c] Intensity average lifetime. [d] Fluorescence rate $k_f = \Phi / <\tau>$.

the photophysical properties (Figure 4a). To ensure the solubility of anions as a Lewis base in THF, tetrabutylammonium (TBA) salts (n-Bu$_4$N$^+$A$^-$) were employed as the source of the Lewis base. When a hard and small or linear-shaped anion such as hydroxide (HO$^-$), acetate (AcO$^-$), cyanate (NCO$^-$), cyanide (CN$^-$), and fluoride (F$^-$) was added, the color of the solution containing **1-Mes** changed from pale yellow to pink (as seen in the inset photograph in Figure 4a). This color change is caused by a distinct red-shift of the absorption spectrum as designed (Figure 4a). The absorbance at 252, 395, and 419 nm decreased, while the absorption band between 280 and 340 nm increased. Additionally, a new broadband emerged in the vicinity of 500 nm (Figure 4a), which is ascribed to the absorption of difluoride adduct of **1-Mes** ([**1-Mes-2F**]$^{2-}$[(n-Bu$_4$N)$_2$]$^{2+}$). Absorption spectrum simulations of the difluoride adduct [**1-Mes-2F**]$^{2-}$ confirmed the presence of a low-intensity band near the 500 nm mark (Figure S15a). Further analysis of the ensemble demonstrates that the S$_0$ to S$_1$ transition of [**1-Mes-2F**]$^{2-}$ displays strong CT character (Figure S16a and b). The addition of a larger anionic species such as chloride (Cl$^-$), bromide (Br$^-$), nitrate (NO$_3^-$), triflate (TfO$^-$), and a neutral Lewis base (e.g., Et$_3$N, pyridine, and DABCO) did not alter the absorption spectrum in any discernible manner (Figure S9a). **1-Tipp** displayed a similar change in absorption spectrum when 60 equiv. of TBAF, TBAOH, and TBACN was added to the solution, although the absorbance of the ICT band (ca. 500 nm) was smaller than the cases of **1-Mes** (Figure 4b). Also, it is noted that the addition of TBOAc and TBOCN did not cause a change in absorption spectra (Figure S9c), probably due to the kinetic and thermodynamic suppression of borate formation by increased steric hindrance around the boron center. Conversely, this difference in anion-responsive behavior demonstrates that the binding of the anion to the boron center modulates photophysical properties. Other n-Bu$_4$N$^+$A$^-$ and neutral amines did not cause a significant change in absorption spectra in a similar manner with **1-Mes** (Figure S9c). Although these experiments were carefully and repeatedly conducted, it is difficult to exclude completely the possibility that the potential hydration of Lewis bases affects the photophysical properties.

In addition to the colorimetric behavior, a significant alteration in PL was observed upon the addition of a Lewis
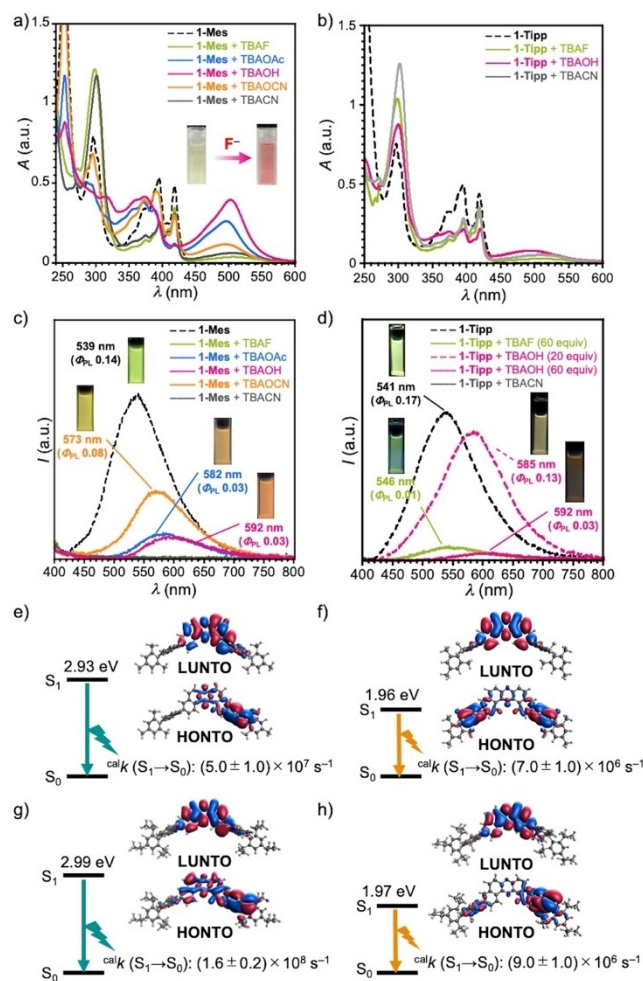

Figure 4. UV/Vis absorption spectra of a) **1-Mes** and b) **1-Tipp** in the absence and presence of a Lewis base (n-Bu$_4$N$^+$A$^-$) in THF ($c = 10^{-5}$ M). 20 and 60 equiv. of n-Bu$_4$N$^+$A$^-$ was added to **1-Mes** and **1-Tipp**, respectively. The inset photograph in a) shows the appearance of solutions of **1-Mes** (0 equiv) and **1-Mes** + TBAF (100 equiv). PL spectra of c) **1-Mes** and d) **1-Tipp** in the absence and presence of a Lewis base (n-Bu$_4$N$^+$A$^-$) in THF. The highest occupied natural transition orbital (HONTO) and lowest unoccupied natural transition orbital (LUNTO) for the S$_1 \rightarrow$ S$_0$ transition of e) **1-Mes**, f) [**1-Mes-2F**]$^{2-}$, g) **1-Tipp**, and h) [**1-Tipp-2F**]$^{2-}$ in 1,4-dioxane.

base capable of forming a complex with **1-Mes** (Figure 4c) in THF. The green emission of **1-Mes** ($\lambda_{em} = 539$ nm) turned to orange ($\lambda_{em} = 592$ nm) upon the addition of HO⁻ (Figure 4c). Similar significant red-shifts in PL were observed in the cases of the addition of AcO⁻ and NCO⁻ (Figure 4c). In contrast, fluoride and cyanide resulted in the quenching of emission ("turn-off" of PL) (Figure 4c). Notably, in 1,4-dioxane, a less polar solvent than THF, the PL of **1-Mes** displayed a significantly red-shifted emission (peak at 590 nm) upon the addition of TBAF (Figure S10a). Fluorescence spectrum simulations (Figure S17) predicted the fluorescence of [**1-Mes-2F**]²⁻ at 634 nm in 1,4-dioxane, which is in good agreement with the experimental results. An estimated emission rate of $(7.0 \pm 1.0) \times 10^6$ s⁻¹ was obtained, a significant reduction when compared with calculated fluorescence rates for compound **1-Mes**, which helps explain the lower measured PL quantum yields (PLQYs) (**1-Mes**: $\Phi_{PL} = 0.24$ *vs* [**1-Mes-2F**]²⁻: $\Phi_{PL} = 0.05$). In the case of **1-Tipp**, the addition of fluoride led to almost quenching of PL (Figure 4d). In a similar manner with **1-Mes**, the addition of TBAOH to the solution of **1-Tipp** led to a significant red-shift in emission as a function of the amount of added anion (λ_{em} 585 nm at 20 equiv; λ_{em} 592 nm at 60 equiv), modulating the emission color (Figure 4d). Also, in 1,4-dioxane, a significant red-shift of PL of **1-Tipp** upon the addition of TBAF was observed (Figure S10b). The requirement of extra amounts of TBAF for **1-Tipp** for the red-shift indicates a smaller binding constant of **1-Tipp** against fluoride when compared with **1-Mes**. Figures 4e and f depict the differences in emission properties and electronic structures of the first excited states of compounds **1-Mes** and [**1-Mes-2F**]²⁻ in 1,4-dioxane. For the emission in THF, simulations pointed at a fluorescence peak at 790 nm with a calculated rate of $(2.6 \pm 0.2) \times 10^6$ s⁻¹ (Figure S17). Emission at such long wavelengths is expected to be strongly quenched by internal conversion, following the energy gap law,[25] which could explain why no emission was observed experimentally in this case. Importantly, the addition of BF₃ to the "turn-off" solution of **1-Mes** recovered the PL in a reversible way ("turn-on") (Figure S11a). The colorimetric change was also reversible upon the same protocol (Figure S11b), indicating that the coordination of fluoride to **1-Mes** is a chemically reversible process. As for **1-Tipp**, the decreased PL was also recovered by the addition of BF₃ (Figure S11c), and a similar colorimetric behavior was observed (Figure S11d). It is also worth noting that the bases that did not show colorimetric change did not exhibit a change in emission either (Figure S9b and d).

The change in chemical species of **1** through the addition of a Lewis base was investigated utilizing NMR spectroscopy (Figure 5 and S24–S27). The addition of fluoride (10 equiv. of TBAF) as a Lewis base to **1-Mes** in THF-d_8 resulted in a significant shift of the aromatic resonances to the higher field region, while preserving the splitting pattern of the signals (Figure 5; the assignment of the ¹H and ¹³C nuclei of [**1-Mes-2F**]²⁻[(n-Bu₄N)₂]²⁺ was conducted by 2D NMR spectroscopic analysis. For the details, see the Figure S24–S26 in the SI). It is noteworthy that the magnitude of the signal shift |Δδ| is considerably larger for the ¹H nuclei attributed
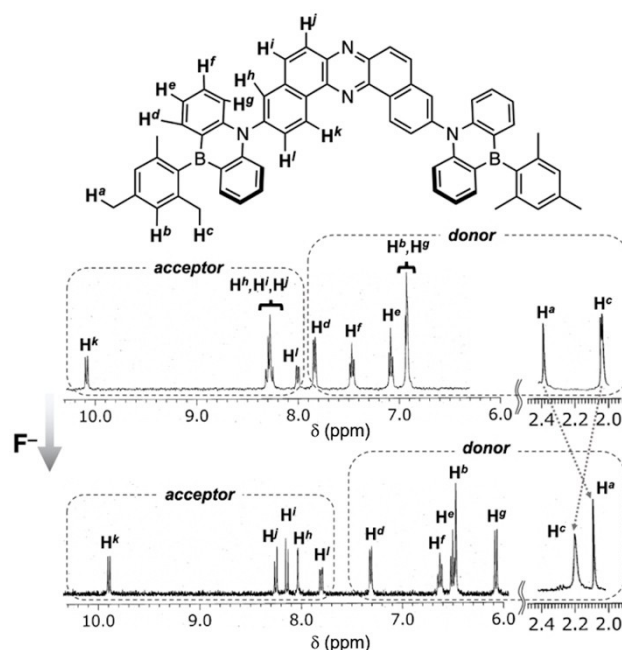

Figure 5. Change in the ¹H NMR spectrum of **1-Mes** upon the addition of fluoride (10 equiv.) in THF-d_8.

to the donor (**Hᵃ**–**Hᵍ** 0.21–0.85 ppm) than those for the acceptor (**Hʰ**–**Hˡ** 0.06–0.24 ppm) (for the detailed values, see Table S6). A similar shift was also observed with **1-Tipp** upon the addition of TBAF (Figure S27). Additionally, it is intriguing to note that only the ¹H nuclei of o-CH_3 of the B-Mes group (**Hᶜ**) of **1-Mes** shifted to the lower field, from 2.0 ppm to 2.2 ppm (Figure 5).[25] Given the proximity of the o-CH_3 and boron-coordinated fluoride on the tetracoordinate boron center (2.40 Å < the sum of Van der Waals radii of H and F: 2.60 Å) in the optimized S_0 geometry, hydrogen bonding H···F could be operative in the adduct [**1-Mes-2F**]²⁻[(n-Bu₄N)₂]²⁺ (Figure S18a).

In order to explore the origin of the substantial upfield-shift of the ¹H nuclei in the donor unit, the nucleus-independent chemical shift (NICS) (1) values of the PAzB and fused benzene ring in the donor unit were investigated by DFT calculations (Figure S19). Whereas the NICS (1) value of the PAzB ring underwent a marked transformation from −4.26 (**1-Mes**) and −4.18 (**1-Tipp**) ppm (aromatic) to +1.00 ([**1-Mes-2F**]²⁻) and +1.81 ([**1-Tipp-2F**]²⁻) ppm (non-aromatic) upon coordination with fluoride at the boron center, the NICS (1) value of the peripheral benzene ring remained unchanged (ranging from −10.66 to −9.90 ppm) (Figure S19). Since the aromaticity of the fused benzene rings did not change upon formation of borate, it can be inferred that the increase in electron density on the donor unit resulting from the action of fluoride led to the significant shift of the donor ¹H nuclei to the higher field region. This hypothesis was further supported by the electrostatic potential (ESP) mapping of **1** and [**1**–**2F**]²⁻ (Figure S20). The presence of a ¹¹B NMR resonance of **1-Mes** at +58.5 ppm (Figure S28a) indicated that compound **1-Mes** has a planar tricoordinate boron center, which is in

consistent with the structure observed by the X-ray crystallographic analysis. Following the addition of fluoride, a new signal appeared at +1.6 ppm, which is indicative of the formation of sp³-hybridized tetracoordinate borate of PAzB [**1-Mes-2F**]²⁻[(*n*-Bu₄N)₂]²⁺ (Figure S28b).[17g]

Cyclic voltammetry (CV) enables the assessment of changes in the HOMO/LUMO energy of the D–A–D compounds. The cyclic voltammogram of **1-Mes** in CH₂Cl₂ revealed a reversible reduction process (${}^{red}E_{onset} = -1.71$ V vs Fc/Fc⁺) and an irreversible oxidation process (${}^{ox}E_{onset} = +0.92$ V vs Fc/Fc⁺) (Figure S29a). The oxidation potential and electrochemical instability of **1-Mes** is similar to that of **N-Ph PAzB-Mes**.[26] The large electrode current in the oxidation process and irreversible behavior are probably ascribed to the electrochemical polymerization at the donor unit on the electrode. The HOMO and LUMO, calculated using the redox potential, are −6.02 eV and −3.39 eV, respectively. The LUMO energy is nearly identical to that of DBPHZ (−3.22 eV),[19] supporting the localization of the HOMO and LUMO on the D and A, respectively. The cyclic voltammogram obtained in the presence of fluoride (TBAF) displayed a drastic negative shift in both the reduction potential (${}^{red}E_{onset} = -2.21$ V vs Fc/Fc⁺) and the oxidation potential (${}^{ox}E_{onset} = -0.61$ V vs Fc/Fc⁺) when compared with **1-Mes** (Figure S29b); the HOMO and LUMO energy of [**1-Mes-2F**]²⁻[(*n*-Bu₄N)₂]²⁺ is estimated to be −4.49 eV and −2.89 eV, respectively. It should be noted that the oxidation potential shifted much more negatively ($\Delta^{ox}E_{onset} = -1.53$ V) than the reduction potential ($\Delta^{red}E_{onset} = -0.50$ V). It further supports the coordination of fluoride to the boron center to form a borate, which is much more easily oxidized, due to an increase in electron density. The theoretically calculated HOMO/LUMO energy levels of **1-Mes** (−5.7 eV/−2.7 eV) and [**1-Mes-2F**]²⁻[(*n*-Bu₄N)₂]²⁺ (−4.3 eV/−2.2 eV) in CH₂Cl₂ (Figure 1e) are qualitatively consistent with the experimental results. In the case of **1-Tipp**, the CV of the neutral molecule gave almost the same voltammogram (${}^{ox}E_{onset} = +0.83$ V; ${}^{red}E_{onset} = -1.67$ V vs Fc/Fc⁺, Figure S29c) with **1-Mes**. Also, a significant negative shift in ${}^{ox}E_{onset}$ (−1.09 V vs Fc/Fc⁺) in the presence of TBAF (400 equiv) was observed (Figure S29c and d), indicating the increase in the HOMO level (−4.84 eV) by coordination of fluoride.

To assess the binding capability of **1** with fluoride, titration experiments were conducted using UV/Vis absorption spectroscopy (Figure 6a and b). The absorption spectrum of **1-Mes** undergoes gradual changes as a function of the amount of TBAF added. As the amount of fluoride added increases, the absorbance at 252, 395, and 419 nm decreases (blue arrow in Figure 6a), while the absorbance at 298 nm increases (red arrows in Figure 6a). It is noteworthy that a new absorption band at approximately 500 nm emerged, which should be ascribed to the absorption of [**1-Mes-2F**]²⁻[(*n*-Bu₄N)₂]²⁺⁻ (and/or [**1-Mes-F**]⁻[*n*-Bu₄N]⁺). Plotting the difference in absorbance at $\lambda_{abs} = 500$ nm (ΔA_{500}) against [F⁻]₀/[**1-Mes**]₀ yields the titration curve (the inset graph in Figure 6a). Although the precise binding constants for fluoride were difficult to determine by the UV/Vis titration, fitting the curve with a non-cooperative 1:2 bind-
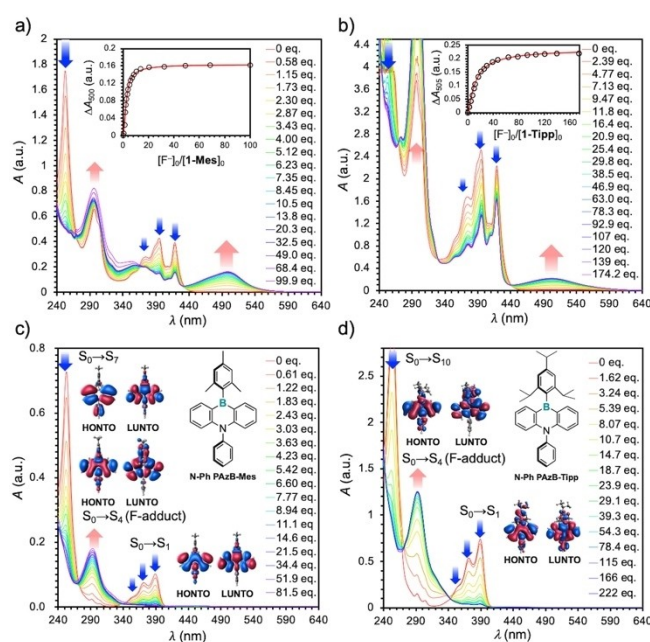

Figure 6. UV/Vis absorption titration spectra of a) **1-Mes** ($c = 1.0 \times 10^{-5}$ M), b) **1-Tipp** ($c = 5.0 \times 10^{-5}$ M) (the insets show titration plots and fitting curves), c) **N-Ph PAzB-Mes** ($c = 1.0 \times 10^{-5}$ M), and d) **N-Ph PAzB-Tipp** ($c = 4.2 \times 10^{-5}$ M) in THF as a function of the amount of TBAF added.

ing model (Figure S30, $K_1 = 4 K_2$)[27,28] produced estimates of $K_1 = (3.31 \pm 0.21) \times 10^5$ M⁻¹ and $K_2 = (0.83 \pm 0.05) \times 10^5$ M⁻¹. It is noteworthy that these values are comparable to those of bridge-atom-free TABs,[4] demonstrating the well-balanced design for Lewis acidic electron donor. Titration of **1-Tipp** with TBAF resulted in a similar change in UV/Vis spectrum (Figure 6b) but revealed that the binding constants extracted from the titration curve are much smaller [$K_1 = (8.46 \pm 0.32) \times 10^3$ M⁻¹ and $K_2 = (2.11 \pm 0.08) \times 10^3$ M⁻¹] than **1-Mes**. This result indicates that the increase in steric bulkiness around the boron center thermodynamically destabilizes the tetrahedral fluoroborate and thus lowers the binding constant.

To investigate the efficacy of the acceptor unit at the nitrogen atom of PAzB on the photophysical change upon the addition of fluoride, *B*-Mes and *B*-Tipp PAzB having an electronically neutral aryl moiety (**N-Ph PAzB-Mes**[29] and **N-Ph PAzB-Tipp**[30]) were titrated with fluoride (Figure 6c and d, for the syntheses, see [Eq. (S5) and (S9)]). Upon addition of fluoride, the vibronic-structured absorptions of **N-Ph PAzB-Mes** between 340 and 405 nm (S₀→S₁ transition with multi-resonance intramolecular CT character) and a sharp strong absorption at 253 nm (S₀→S₇ transition with π-π* character) decreased, and there was a rise of absorption at 293 nm (S₀→S₄ transition of the corresponding fluoroborate with π-π* and CT character) (Figure 6c and d, Figure S21–S23). As a whole, the absorption spectra were blue-shifted, as commonly observed with TABs.[4] Comparison of the photophysical behavior of **1-Mes** and **N-Ph PAzB-Mes** clearly showcases that significant red-shift in the absorption spectrum of **1-Mes** upon addition of fluoride is ascribed to the presence of acceptor unit at the nitrogen atom of PAzB

structure. The binding constants of **N-Ph PAzB-Mes** and **N-Ph PAzB-Tipp** for fluoride in THF were extracted from the titration curve obtained with the absorbance at $\lambda = 390$ nm (**N-Ph PAzB-Mes**) and 389 nm (**N-Ph PAzB-Tipp**) (Figure S31) to be $K = (7.03 \pm 0.63) \times 10^4$ M^{-1} and $K = (3.15 \pm 0.91) \times 10^3$ M^{-1}, respectively. These values are one order lower than those of **1-Mes** and **1-Tipp**, respectively. Comparing **N-Ph PAzB-Mes** and **N-Ph PAzB-Tipp**, a steric effect on the binding constant was again recognized. The drastic increase in binding constants of **1** when compared with **N-Ph PAzB** can be attributed to the inductive electron-withdrawing effect of the DBPHZ unit as designed. From these titration experiments, we can deduce that the minimum detection limit of fluoride in THF with **1-Mes** and **1-Tipp** are at least 1.52 ± 0.05 ppm (5.81 ± 0.18 μM) and 3.29 ± 0.22 ppm (11.9 ± 0.15 μM), respectively.

To explore the feasibility of utilizing D–A–D compounds **1** for solid-state applications, we examined its solid-state properties. Since **1-Mes** has a much higher affinity toward fluoride than **1-Tipp**, **1-Mes** was selected for this application. Compound **1-Mes** displays green emission ($\lambda_{em} = 511$ nm, $\Phi_{PL} = 0.14$) in the solid state (Figure S32a). Compared to a dilute solution of **1-Mes** in cyclohexane ($\lambda_{em} = 440$ nm, $\Phi_{PL} = 0.23$), the emission peak is slightly red-shifted by 3158 cm^{-1} and the PLQY is lower ($\Phi_{PL} = 0.14$). It suggests that, despite its orthogonal D–A–D molecular geometry, some electronic interactions between molecules are operative in the solid state, as evidenced by the X-ray crystallographic analysis (Figure S4), leading to slight aggregation-caused quenching (ACQ). Compound **1-Tipp** showed blue-shifted PL with a lower PLQY ($\Phi_{PL} = 0.09$).

The success in enhancing the CT process of compound **1-Mes** in solution through Lewis acid-base interactions prompted us to investigate its solid-state application of modulating emission colors through the fabricating process. Spin-coating a mixture of **1-Mes** (1 wt %) and a polymer matrix in an organic solvent onto a quartz plate, followed by drying under vacuum, resulted in a film (for the detailed procedure, see the SI). The polystyrene (PS) and poly(methyl methacrylate) (PMMA) films containing **1-Mes** displayed blue ($\lambda_{em} = 465$ nm, $\Phi_{PL} = 0.20$) and green ($\lambda_{em} = 535$ nm, $\Phi_{PL} = 0.15$) emission, respectively (Figure 7a). Similar to solvatochromism in solution, the polar matrix enables emission in the lower energy regime, due to the stabilization of the ^{1}CT state in the excited state. Notably, the films fabricated from the mixture of **1-Mes**, TBAF, and a matrix displayed a distinct red-shift in PL spectra when compared with polymer films containing only **1-Mes** (shift in wavenumber is 5402 cm^{-1} for PS film; 4072 cm^{-1} for PMMA film, Figure 7a), indicating the preservation of fluoroborate [**1-Mes-2F**]$^{2-}$[(n-Bu$_4$N)$_2$]$^{2+}$ even in the matrix. It should be noted that the PL was not quenched in the matrix, probably due to the suppression of molecular vibration in the rigid environment. Additionally, it should be noted that the emission of **1-Mes** + TBAF in PMMA film was observed in the deep-red to NIR region with a moderately good PLQY among reported purely organic NIR emitters, which have recently found new applications such as security authentication and optical imaging (Figure 7a).[31] Further modulation
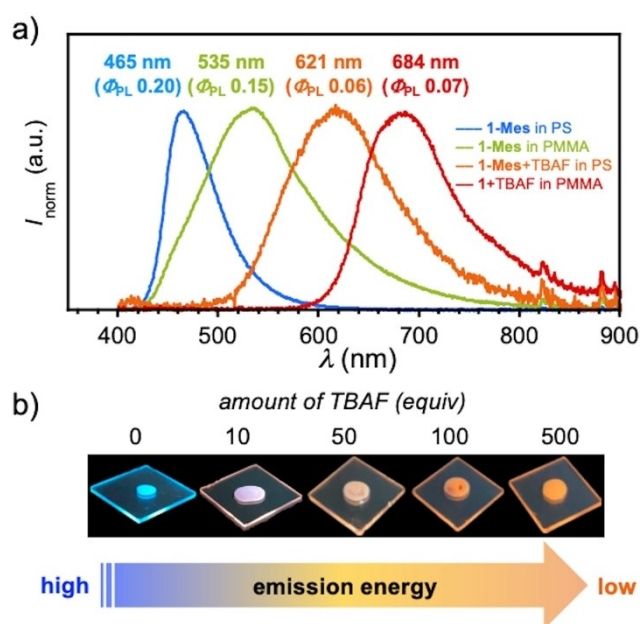

Figure 7. a) PL spectra of **1-Mes** (1 wt %) in PS (in sky-blue), **1-Mes** in PMMA (in moth green), **1-Mes** + TBAF (500 equiv) in PS (in orange), and **1-Mes** + TBAF (100 equiv) in PMMA films ($\lambda_{ex} = 365$ nm); b) photographs of **1-Mes** with varied TBAF content in PS films taken under the irradiation of a UV lamp ($\lambda_{ex} = 365$ nm).

of photophysical properties of **1-Mes** was implemented by varying the equivalent of TBAF for fabricating films (Figure 7b and Figure S33). The PL spectrum of the film gradually transformed from a single peaked Gaussian-type shape in the blue region to a dual peaked emission as a function of the amount of TBAF added (Figure S33). Specifically, it is noted that the PS film fabricated from **1-Mes** + 10 equivalents of TBAF exhibited warm white light and its *Commission International de l'Eclairage* (CIE) is (0.39, 0.33). Implementation of white emission with a single fluorophore can serve as a promising approach for optoelectronics and sensors.[32] In the presence more than 50 equivalents of TBAF, the redder emission at around 570 nm further red-shifted to 625 nm. The PL intensity ratio of blue to orange emission decreased, and the film containing 500 equivalents of TBAF displayed a single Gaussian-type PL emission at λ_{em} 621 nm (Figure S33). By making use of change in PL spectrum, the emission color of the film is tunable (Figure 7b). Since the emission in the blue region ascribed to D–A–D compound **1-Mes** is overlapped with the excitation spectrum of the film fabricated with **1-Mes** + TBAF (Figure S34), the Förster resonance energy transfer (FRET) would be operative to lead to significant red-shifted emission from the admixture of **1-Mes** and its borates.

Conclusion

In conclusion, novel triarylboranes **1** that exhibit a red-shift in both their absorption and PL spectra in response to anionic species have been developed. This achievement was

accomplished by judiciously reconciling the dualistic properties of PAzB as both an electron donor and a Lewis acid. Coordination of anionic species to the boron center resulted in a marked enhancement of the HOMO energy, which in turn led to a reduction in the HOMO–LUMO gap and the subsequent colorimetric red-shift. Additionally, the strong interaction with fluoride ions facilitates an enhancement in the charge-transfer character of the excited state, leading to a red-shift in the PL in solution and the solid state. This novel approach holds promise for modulating the photophysical properties of triarylborane-based organic materials.

Conflict of Interest

The authors declare no conflict of interest.

Data Availability Statement

The data that support the findings of this study are available in the supplementary material of this article.

Keywords: boron · donor-acceptor · charge-transfer · luminescence · sensor

[1] A. Suzuki, *Organoboranes in Organic Syntheses*, Hokkaido University Press, Sapporo, **2010**.

[2] J. L. Carden, A. Dasgupta, R. L. Melen, *Chem. Soc. Rev.* **2020**, *49*, 1706–1725.

[3] a) C. D. Entwistle, T. B. Marder, *Angew. Chem. Int. Ed.* **2002**, *41*, 2927–2931; b) C. D. Entwistle, T. B. Marder, *Chem. Mater.* **2004**, *16*, 4574–4585; c) S. Mukherjee, P. Thilagar, *J. Mater. Chem. C* **2016**, *4*, 2647–2662; d) S. M. Berger, T. B. Marder, *Mater. Horiz.* **2022**, *9*, 112–120, and references therein.

[4] a) T. W. Hudnall, C.-W. Chiu, F. P. Gabbaï, *Acc. Chem. Res.* **2009**, *42*, 388–397; b) C. R. Wade, A. E. J. Broomsgrove, S. Aldridge, F. P. Gabbaï, *Chem. Rev.* **2010**, *110*, 3958–3984.

[5] S. Yamaguchi, S. Akiyama, K. Tamao, *J. Am. Chem. Soc.* **2001**, *123*, 11372–11375.

[6] S. Yamaguchi, T. Shirasaka, S. Akiyama, K. Tamao, *J. Am. Chem. Soc.* **2002**, *124*, 8816–8817.

[7] M. Miyata, Y. Chujo, *Polym. J.* **2002**, *34*, 967–969.

[8] A. Sundararaman, M. Victor, R. Varughese, F. Jäkle, *J. Am. Chem. Soc.* **2005**, *127*, 13748–13749.

[9] K. Parab, K. Venkatasubbaiah, F. Jäkle, *J. Am. Chem. Soc.* **2006**, *128*, 12879–12885.

[10] Y. Kubo, M. Yamamoto, M. Ikeda, M. Takeuchi, S. Shinkai, S. Yamaguchi, K. Tamao, *Angew. Chem. Int. Ed.* **2003**, *42*, 2036–2040; *Angew. Chem.* **2003**, *115*, 2082–2086.

[11] a) Z.-Q. Liu, M. Shi, F.-Y. Li, Q. Fang, Z.-H. Chen, T. Yi, C.-H. Huang, *Org. Lett.* **2005**, *7*, 5481–5484; b) M.-S. Yuan, Z.-Q. Liu, Q. Fang, *J. Org. Chem.* **2007**, *72*, 7915–7922.

[12] a) X. Y. Liu, D. R. Bai, S. Wang, *Angew. Chem. Int. Ed.* **2006**, *45*, 5475–5478; *Angew. Chem.* **2006**, *118*, 5601–5604; b) D.-R. Bai, X.-Y. Liu, S. Wang, *Chem. Eur. J.* **2007**, *13*, 5713–5723.

[13] G. Zhou, M. Baumgarten, K. Müllen, *J. Am. Chem. Soc.* **2008**, *130*, 12477–12484.

[14] a) S. Solé, F. P. Gabbaï, *Chem. Commun.* **2004**, *4*, 1284–1285; b) M. Melaimi, F. P. Gabbaï, *J. Am. Chem. Soc.* **2005**, *127*, 9680–9681; c) A. Sundararaman, K. Venkatasubbaiah, M. Victor, L. N. Zakharov, A. L. Rheingold, F. Jäkle, *J. Am. Chem. Soc.* **2006**, *128*, 16554–16565; d) T. W. Hudnall, M. Melaïmi, F. P. Gabbaï, *Org. Lett.* **2006**, *8*, 2747–2749; e) S.-B. Zhao, T. McCormick, S. Wang, *Inorg. Chem.* **2007**, *46*, 10965–10967; f) Y. Sun, N. Ross, S.-B. Zhao, K. Huszarik, W.-L. Jia, R.-Y. Wang, D. Macartney, S. Wang, *J. Am. Chem. Soc.* **2007**, *129*, 7510–7511; g) T. W. Hudnall, F. P. Gabbaï, *J. Am. Chem. Soc.* **2007**, *129*, 11978–11986; h) C.-W. Chiu, Y. Kim, F. P. Gabbaï, *J. Am. Chem. Soc.* **2009**, *131*, 60–61; i) Y. Kim, F. P. Gabbaï, *J. Am. Chem. Soc.* **2009**, *131*, 3363–3369; j) T. Matsumoto, C. R. Wade, F. P. Gabbaï, *Organometallics* **2010**, *29*, 5490–5495; k) H. Zhao, F. P. Gabbaï, *Organometallics* **2012**, *31*, 2327–2335; l) K. C. Song, K. M. Lee, N. Van Nghia, W. Y. Sung, Y. Do, M. H. Lee, *Organometallics* **2013**, *32*, 817–823; m) D.-M. Chen, S. Wang, H.-X. Li, X.-Z. Zhu, C.-H. Zhao, *Inorg. Chem.* **2014**, *53*, 12532–12539; n) A. L. Brazeau, K. Yuan, S.-B. Ko, I. Wyman, S. Wang, *ACS Omega* **2017**, *2*, 8625–8632; o) P. Li, D. Shimoyama, N. Zhang, Y. Jia, G. Hu, C. Li, X. Yin, N. Wang, F. Jäkle, P. Chen, *Angew. Chem. Int. Ed.* **2022**, *61*, e202200612; *Angew. Chem.* **2022**, *134*, e202200612.

[15] a) T. Neumann, Y. Dienes, T. Baumgartner, *Org. Lett.* **2006**, *8*, 495–497; b) C. R. Wade, F. P. Gabbaï, *Dalton Trans.* **2009**, 9169–9175; c) H. Li, F. Jäkle, *Angew. Chem. Int. Ed.* **2009**, *48*, 2313–2316; *Angew. Chem.* **2009**, *121*, 2349–2352; d) C. A. Swamy P, R. N. Priyanka, S. Mukherjee, P. Thilagar, *Eur. J. Inorg. Chem.* **2015**, 2338–2344; e) G. R. Kumar, S. K. Sarkar, P. Thilagar, *Chem. Eur. J.* **2016**, *22*, 17215–17225; f) R. E. Messersmith, S. Yadav, M. A. Siegler, H. Ottosson, J. D. Tovar, *J. Org. Chem.* **2017**, *82*, 13440–13448; g) G. Turkoglu, M. E. Cinar, T. Ozturk, *Eur. J. Org. Chem.* **2017**, 4552–4561.

[16] In the same timeline as our work, Danos and Zysman-Colman et al. independently reported that phenazaborine serves as a weak electron donor in a donor–acceptor conjugated emitter: P. Sudhakar, S. Kuila, K. Stavrou, A. Danos, A. M. Z. Slawin, A. Monkman, E. Zysman-Colman, *ACS Appl. Mater. Interfaces* **2023**, *15*, 25806–25818.

[17] a) P. M. Maitlis, *J. Chem. Soc.* **1961**, 425–429; b) M. Kranz, F. Hampel, T. Clark, *J. Chem. Soc. Chem. Commun.* **1992**, 1247–1248; c) T. Agou, J. Kobayashi, T. Kawashima, *Org. Lett.* **2006**, *8*, 2241–2244; d) T. Agou, J. Kobayashi, T. Kawashima, *Chem. Commun.* **2007**, 3204–3206; e) T. Agou, T. Kojima, J. Kobayashi, T. Kawashima, *Org. Lett.* **2009**, *11*, 3534–3537; f) T. Agou, M. Sekine, J. Kobayashi, T. Kawashima, *Chem. Eur. J.* **2009**,

Angew. Chem. Int. Ed. **2024**, e202405158 (9 of 10)

© 2024 The Authors. Angewandte Chemie International Edition published by Wiley-VCH GmbH

15, 5056–5062; g) T. Agou, M. Sekine, J. Kobayashi, T. Kawashima, *Chem. Commun.* **2009**, 1894–1896; h) T. Agou, H. Arai, T. Kawashima, *Chem. Lett.* **2010**, *39*, 612–613; i) Y. Ishikawa, K. Suzuki, K. Hayashi, S.-Y. Nema, M. Yamashita, *Org. Lett.* **2019**, *21*, 1722–1725.

[18] T. Agou, J. Kobayashi, T. Kawashima, *Inorg. Chem.* **2006**, *45*, 9137–9144.

[19] Y. Takeda, M. Okazaki, S. Minakata, *Chem. Commun.* **2014**, *50*, 10291–10294.

[20] a) P. Data, P. Pander, M. Okazaki, Y. Takeda, S. Minakata, A. P. Monkman, *Angew. Chem. Int. Ed.* **2016**, *55*, 5739–5744; *Angew. Chem.* **2016**, *128*, 5833–5838; b) H. F. Higginbotham, M. Okazaki, P. de Silva, S. Minakata, Y. Takeda, P. Data, *ACS Appl. Mater. Interfaces* **2021**, *13*, 2899–2907.

[21] J. A. Knöller, G. Meng, X. Wang, D. Hall, A. Pershin, D. Beljonne, Y. Olivier, S. Laschat, E. Zysman-Colman, S. Wang, *Angew. Chem. Int. Ed.* **2020**, *59*, 3156–3160; *Angew. Chem.* **2020**, *132*, 3181–3185.

[22] W.-M. Wan, F. Cheng, F. Jäkle, *Angew. Chem. Int. Ed.* **2014**, *53*, 8934–8938; *Angew. Chem.* **2014**, *126*, 9080–9084.

[23] Deposition Numbers 2237690 (for **1-Mes**) and 2328443 (for **1-Tipp**) contain the supplementary crystallographic data for this paper. These data are provided free of charge by the joint Cambridge Crystallographic Data Centre and Fachinformationszentrum Karlsruhe Access Structures service.

[24] a) L. E. de Sousa, P. de Silva, *J. Chem. Theory Comput.* **2021**, *17*, 5816–5824; b) L. E. de Sousa, P. de Silva, *J. Phys. Chem. A* **2023**, *127*, 8200–8208.

[25] K. F. Freed, *Acc. Chem. Res.* **1978**, *11*, 74–80.

[26] T. Agou, J. Kobayashi, Y. Kim, F. P. Gabbaï, T. Kawashima, *Chem. Lett.* **2007**, *36*, 976–977.

[27] P. Thordarson, *Chem. Soc. Rev.* **2011**, *40*, 1305–1323.

[28] http://app.supramolecular.org/bindfit/.

[29] M. Ando, M. Sakai, N. Ando, M. Hirai, S. Yamaguchi, *Org. Biomol. Chem.* **2019**, *17*, 5500–5504.

[30] M. Kondo, T. Agou, *Chem. Commun.* **2022**, *58*, 5001–5004.

[31] M.-P. Zhuo, X.-D. Wang, L.-S. Liao, *Small Sci.* **2022**, *2*, 2200029.

[32] Z. Chen, C.-L. Ho, L. Wang, W.-Y. Wong, *Adv. Mater.* **2020**, *32*.

Research Articles

Donor-Acceptor Systems

N. Aota, R. Nakagawa, L. E. de Sousa,
N. Tohnai, S. Minakata, P. de Silva,*
Y. Takeda* ———————— **e202405158**

Anion-Responsive Colorimetric and Fluoro-
metric Red-Shift in Triarylborane Deriva-
tives: Dual Role of Phenazaborine as Lewis
Acid and Electron Donor

Lewis acid point · CT · electron donor
· red-shift in absorption/emission · modulation of solid-state emission
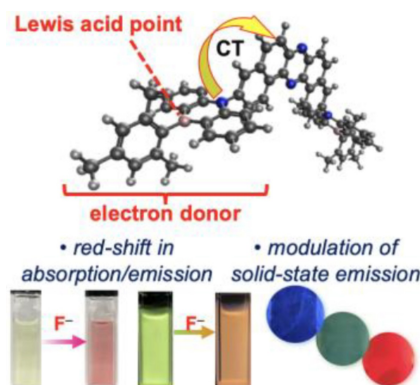
A strategy of modulating photophysical properties by balancing the contradictory role of phenazaborine as a Lewis acid and an electron donor has been used to synthesize anion-responsive triarylborane compounds that displayed significant red-shift in their absorption and photoluminescence spectra in solution. This approach has also been successfully applied to modulate the emission color in polymer films.